Rayleigh-Taylor Instability in a Finite Cylinder: Linear Stability Analysis and Long Time Fingering Solutions

H. SWEENEY,[1] R. R. KERSWELL [1] AND T. MULLIN [2]

[1]School of Mathematics, University of Bristol, Bristol BS8 1TW, UK
[2]School of Physics and Astronomy, University of Manchester. Manchester M13 9PL, UK

(Received 13 September 2013)

We consider the Rayleigh-Taylor instability problem of two initially stationary immiscible viscous fluids positioned with the denser above the less dense in a finite circular cylinder such that their starting fluid-fluid interface is the horizontal midplane of the cylinder. The ensuing linear instability problem has a 5D parameter space - defined by the density ratio, the viscosity ratio, the cylinder aspect ratio, the surface tension between the fluids and the ratio of viscous to gravitational timescales - of which we explore only part motivated by recent experiments where viscous fluids exchange in vertical tubes (Beckett et al. 2011). We find that for these experiments, the instability is invariably 'side-by-side' (of azimuthal wavenumber 1 type) but we also uncover parameter regions where the preferred instability is axisymmetric. The fact that both 'core-annular' (axisymmetric) and 'side-by-side' (asymmetric) long-time flows are seen experimentally highlights the fact that the initial Rayleigh-Taylor instability of the interface does not determine the long-time flow configuration in these situations. Finally, long-time flow solutions are presented on the basis they will be slowly-varying fingering solutions.

1. Introduction

The Rayleigh-Taylor instability in which a denser layer of fluid supported by a less dense fluid is gravitationally unstable (Rayleigh 1883) or, equivalently, when a less-dense fluid is accelerated towards a denser fluid (Taylor 1950) is a classic result in fluid mechanics (see the reviews by Sharp 1984 and Abarzhi 2010). It is now well known to have applications throughout geophysics (e.g. Whitehead & Luther 1975), astrophysics (e.g. Arnett et al. 1989) and industry (e.g. Lindl et al. 1992, Hinds et al. 2002) and so continues to attract active study. In text books, the basic phenomenon is usually illustrated for two immiscible inviscid fluids either in a planar (Chandrasekhar 1961, section 92) or cylindrical geometry (problem 1.12 in Drazin & Reid 1981, see Yih 1980, p220, who describes James Clerk Maxwell's interest in this problem, and more recently Yu & Livescu 2008 who treat compressible fluids). It is relatively straightforward to add the effects of viscosity to the planar analysis (Bellman & Pennington 1954, see also Chandrasekhar 1961, section 94) where there are no lateral boundaries. With lateral boundaries, however, Fourier analysis is no longer possible and the subsequently more involved linear stability problem seems to have gone untreated. The main objective here is to remedy this omission at least for a circular cylinder of finite radius and height and two immiscible fluids. The parameter regime of particular interest is that in which the wavelength of the Rayleigh-Taylor instability is comparable to the cylindrical radius so that the main

question is whether the preferred instability is axisymmetric or not. Related work for a continuously stratified fluid in an infinitely long cylinder (Wooding 1959, Batchelor & Nitsche 1993) and the miscible problem where the interface is smeared out (Vanaparthy et al. 2003, 2008) all indicate that the preferred initial instability invariably has an azimuthal wavenumber of one (see Vanaparthy et al. 2003 for a discussion of accompanying numerical and experimental work in that problem). One aim here will be to see if this conclusion carries over to the immiscible fluid problem.

Our particular motivation for pursuing this calculation is to help interpret recent experimental work (Stevenson & Blake 1998, Arakeri et al 2000, Huppert & Hallworth 2007, Beckett et al. 2011) which examined how two fluids of different densities displace each other in a vertical cylinder when released from an unstable initial configuration (e.g. a flat interface at the cylinder midplane with denser fluid over the less dense fluid). The results of Beckett et al. (2011) are particularly interesting in that more than one type of solution is observed depending on the exact density and viscosity ratios of the two fluids. They find that for fluids with a small viscosity ratio ($\lesssim O(100)$), the flow typically asymptotes to an axially-independent 'side-by-side' state where each fluid hugs a side of the tube so that their interface starts and finishes at the tube wall. For larger viscosity ratios, however, the late time flow takes an axially-independent axisymmetric 'core annular' form with the less dense fluid ascending in the core and the more dense descending around the outside so that their interface is a closed circle concentric with the tube. A natural question is whether the initial Rayleigh-Taylor instability dictates the form of the long-time solution with an axisymmetric mode leading to the axisymmetric core-annular flow and the azimuthal wavenumber one mode leading to the asymmetric side-by-side flow. Unfortunately, the answer to this question is unclear from past experimental work either because the focus was solely on long-time solutions (Stevenson & Blake 1998, Arakeri et al. 2000, Huppert & Hallworth 2007) or the experimental set up was not designed to allow observation of the initial interface (Beckett et al. 2011). Our purpose here is to perform the formal theoretical stability analysis so that what should be expected can be compared to the reported experimental observations of long-time solutions to see if there is any correlation.

We also explore 'fingering' solutions which plausibly are the long-time limit of either the side-by-side or core-annular instability. In these, the fluid-fluid interface is assumed over time to have developed a long (compared to the cylindrical radius) but finite finger either attached to the tube wall (the side-by-side case) or not (the core-annular case) so that slow variation along the tube is a valid approximation except at the ends of the flow. It is a relatively simple and logical step to take the steady, axially-independent (2D) exchange flows calculated by Kerswell (2011) and add this slow variation in the axial direction. The key testable prediction made is then the speed at which these 'fingers' move. If this prediction works well, the buoyancy in the bulk of the finger dominates the end effects and drives the flow. A poor prediction, however, suggests that the end effects, where the finger is not slowly varying, are significant.

The plan of the paper is as follows. Section 2 formulates the stability problem of two immiscible fluids, the denser fluid sitting on top of the less dense fluid, in a finite cylinder with its axis aligned with gravity. Section 3 describes the experimental methodology pursued to complement the theoretical developments. Section 4 details the results and discusses how they fit with the work of Stevenson & Blake (1998) and Beckett et al (2011). Then section 5 constructs fingering solutions which slowly vary along the cylindrical axis and compares their propagation speeds with past experimental data and some experiments carried here. A discussion follows in section 6.

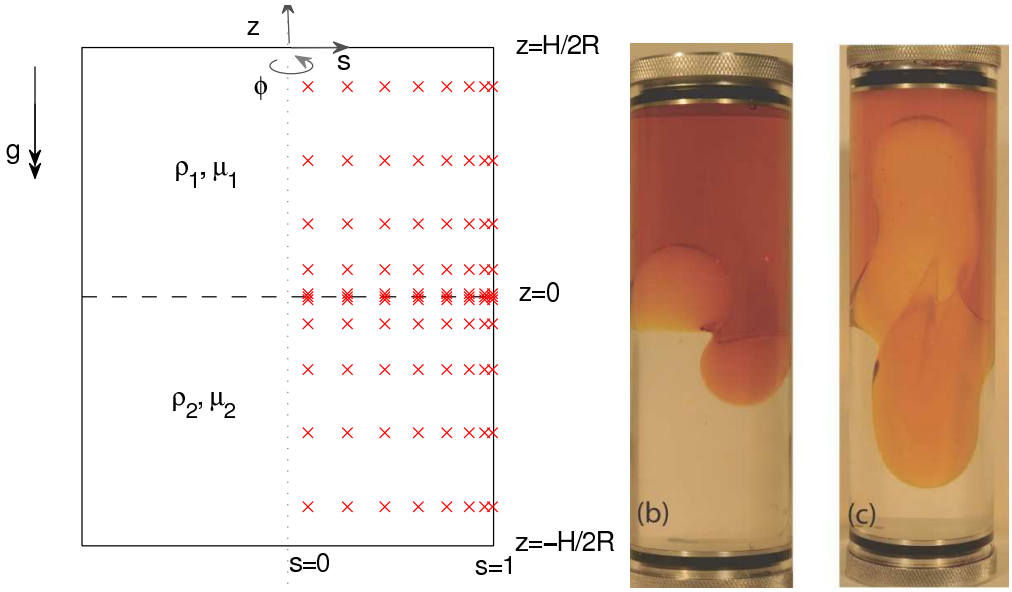

FIGURE 1. Left: the set up with the interface between the two fluids initially horizontal and at $z = 0$. The crosses indicate illustrative collocation points for $L = 8$ and $N = 5$ used in the numerical formulation (Appendix A) to show how they are concentrated in the regions where the flow should vary most (interface and walls). Right: a typical experiment with golden syrup ($\rho_1 = 1.5g/cm^3$, $\mu_1/\rho_1 = 1000cm^2/s$) overlaying silicone oil ($\rho_2 = 0.98g/cm^3$, $\mu_2/\rho_2 = 600cm^2/s$) in a cylinder of radius $3.15cm$ and aspect ratio 5 ($\beta = 0.39$). (b) The side-by-side instability after one second and (c) the complex flow field after 3.5 seconds where the flow becomes axisymmetric - see supplementary material for a video.

2. Formulation

We consider a cylinder of radius R and height H with its axis aligned with gravity $-g\hat{\mathbf{z}}$ containing two immiscible, incompressible, Newtonian fluids of differing densities ρ_1, ρ_2 ($\rho_1 > \rho_2$) and viscosities μ_1, μ_2 initially at rest. The more-dense fluid (subscript 1) occupies the upper half of the cylinder ($0 \leqslant z \leqslant H/2$) and the less-dense fluid (subscript 2) the lower half ($-H/2 \leqslant z < 0$): see figure 1. The Navier-Stokes equations and incompressibility condition

$$\rho_i \left(\frac{\partial \mathbf{U}_i}{\partial t} + \mathbf{U}_i.\nabla\mathbf{U}_i \right) = -\nabla P_i + \mu_i \nabla^2 \mathbf{U}_i - \rho_i g \hat{\mathbf{z}}, \tag{2.1}$$

$$\nabla.\mathbf{U}_i = 0 \tag{2.2}$$

hold for both fluids ($i = 1, 2$). Working in cylindrical coordinates $[Rs, \phi, Rz]$ (so $s \in [0, 1]$ and $z \in [-H/2R, H/2R]$), we let $R\xi(s, \phi, t)$ represent the height of the interface between the two fluids above the midplane. The stationary but gravitationally-unstable starting solution is then

$$\mathbf{U}_1(s, \phi, z) = \mathbf{U}_2(s, \phi, z) = \mathbf{0}, \qquad \xi(s, \phi) = 0, \qquad P_i = -\rho_i g z \tag{2.3}$$

where, crucially, at the interface $z = 0$, the pressure is continuous but not the pressure gradient. Introducing small velocity perturbations of the form $\sqrt{gR}\,\mathbf{u}_i(s, \phi, z, t) = \sqrt{gR}\,(u_i\hat{\mathbf{s}} + v_i\hat{\phi} + w_i\hat{\mathbf{z}})$ and pressure perturbations of the form $\rho_1 g\, p_i(s, \phi, z, t)$ and mea-

suring time in units of $\sqrt{R/g}$ leads to the following linearised equations

$$\frac{\partial \mathbf{u}_1}{\partial t} = -\nabla p_1 + \frac{1}{Re}\nabla^2 \mathbf{u}_1 \qquad z \geqslant 0, \tag{2.4}$$

$$\frac{\partial \mathbf{u}_2}{\partial t} = -\frac{1}{\alpha}\nabla p_2 + \frac{\beta}{\alpha Re}\nabla^2 \mathbf{u}_2 \qquad z < 0 \tag{2.5}$$

along with

$$\nabla.\mathbf{u}_1 = \nabla.\mathbf{u}_2 = 0 \tag{2.6}$$

where

$$\alpha := \frac{\rho_2}{\rho_1}, \quad \beta := \frac{\mu_2}{\mu_1}, \quad \& \quad Re := \frac{\rho_1 R(Rg)^{1/2}}{\mu_1} = \frac{\rho_1 R^2/\mu_1}{\sqrt{R/g}} \tag{2.7}$$

so that the Reynolds number is a ratio of viscous-to-free-fall timescales. (Note that the Atwood number

$$A := \frac{\rho_1 - \rho_2}{\rho_1 + \rho_2} = \frac{1-\alpha}{1+\alpha}.) \tag{2.8}$$

The boundary conditions on the cylinder walls are non-slip

$$\mathbf{u}_1(1, \phi, z \geqslant 0) = \mathbf{0}, \qquad \mathbf{u}_1(s, \phi, +H/2R) = \mathbf{0}, \tag{2.9}$$

$$\mathbf{u}_2(1, \phi, z < 0) = \mathbf{0}, \qquad \mathbf{u}_2(s, \phi, -H/2R) = \mathbf{0} \tag{2.10}$$

and the velocities are continuous at the interface which, to leading order, means

$$\mathbf{u}_1(s, \phi, 0) = \mathbf{u}_2(s, \phi, 0). \tag{2.11}$$

Fluid particles on the interface are assumed to remain there resulting in the normal kinematic condition

$$\frac{D}{Dt}(z - \xi) = 0\Big|_{z=\xi}. \tag{2.12}$$

Taking only leading order terms, this becomes

$$\mathbf{u}_i.\nabla z|_{z=0} = w_i|_{z=0} = \frac{\partial \xi}{\partial t}. \tag{2.13}$$

Continuity of tangential stress requires, to leading order,

$$\left[\left(\frac{\partial v_1}{\partial z} + \frac{1}{s}\frac{\partial w_1}{\partial \phi}\right) - \beta\left(\frac{\partial v_2}{\partial z} + \frac{1}{s}\frac{\partial w_2}{\partial \phi}\right)\right]\Bigg|_{z=0} = 0, \tag{2.14}$$

$$\left[\left(\frac{\partial u_1}{\partial z} + \frac{\partial w_1}{\partial s}\right) - \beta\left(\frac{\partial u_2}{\partial z} + \frac{\partial w_2}{\partial s}\right)\right]\Bigg|_{z=0} = 0. \tag{2.15}$$

With surface tension present, there can be a jump in normal stress at the interface which, again at leading order, implies

$$\left[-(-\xi + p_1) + \frac{2}{Re}\frac{\partial w_1}{\partial z}\right]_{z=0} - \left[-(-\alpha\xi + p_2) + \frac{2\beta}{Re}\frac{\partial w_2}{\partial z}\right]_{z=0} = -T\nabla^2\xi, \tag{2.16}$$

where the (dimensional) surface tension is $\rho_1 g R^2 T$. This condition includes the underlying pressure gradient which is how gravity enters into the linear stability problem. The surface deformation may be eliminated from the problem by utilising the kinematic condition to leave the revised normal stress condition

$$\frac{\partial}{\partial t}\left[p_2 - p_1 + \frac{2}{Re}\left(\frac{\partial w_1}{\partial z} - \beta\frac{\partial w_2}{\partial z}\right)\right]_{z=0} = -T\nabla^2 w + w(\alpha - 1)\Big|_{z=0}. \tag{2.17}$$

α	H/R	T	
0.750	5	0	Fig 5
0.891	2	0	Fig 6a
0.891	5	0	Fig 2
0.891	10	0	Fig 6b
0.891	5	1×10^{-3}	Fig 6c
0.891	5	4×10^{-3}	Fig 6d

TABLE 1. Parameter settings for detailed study. For all, β is varied from 0.001 to 100 and Re from 0.1 to 500.

The linear stability problem consists of solving the equations (2.4)-(2.6) subject to (2.9)-(2.11), (2.14),(2.15) and (2.17).

Given that this system is linear, invariant under shifts in time and has $O(2)$ symmetry in ϕ (invariant under shifts and reflections), the time and azimuthal dependence may be separated off as follows

$$\begin{bmatrix} u_i \\ v_i \\ w_i \\ p_i \end{bmatrix} (s, \phi, z, t) = \begin{bmatrix} \bar{u}_i(s,z)\cos m\phi \\ \bar{v}_i(s,z)\sin m\phi \\ \bar{w}_i(s,z)\cos m\phi \\ \bar{p}_i(s,z)\cos m\phi \end{bmatrix} e^{\lambda t}. \tag{2.18}$$

This leaves a 2 dimensional real eigenvalue problem for $(\bar{\mathbf{u}}_i(s,z), \bar{p}_i(s,z))$ which also produces real eigenvalues (physically, no oscillatory perturbations are expected). The largest λ_m over all m, where

$$\lambda_m := \text{the largest eigenvalue at a given azimuthal wavenumber } m, \tag{2.19}$$

indicates the fastest growing (preferred) instability. The parameter space is 5-dimensional defined by the cylindrical geometry (the aspect ratio H/R), the density ratio ($\alpha = \rho_2/\rho_1$), the viscosity ratio ($\beta = \mu_2/\mu_1$), the ratio of viscous and gravitational timescales (Re, estimated using the denser fluid) and the surface tension (T). This means that an exhaustive exploration is prohibitively expensive. However, sampling a few representative values of the density difference α, surface tension T and geometry H/R while sweeping across β and Re is manageable and proves sufficient for our objectives here. The numerical (spectral) method used to treat the eigenvalue problem is briefly outlined in Appendix A. This code was tested by treating the case of a cylinder of finite radius but infinite height and where the boundary conditions on the sidewalls are changed slightly (see Appendix B). It turns out that in this situation, the Rayleigh-Taylor problem boils down to finding where the determinant of a 4×4 matrix vanishes. Taking $H/R = 20$ in the finite cylinder code proves sufficient to recover the 'exact' determinant results to at least 7 digit accuracy: see Table 2 in Appendix B.

3. Experiments

The apparatus used in our experiments was simple in concept but carefully constructed using specifically manufactured high precision glass and acrylic tubes to ensure repeatable results. One set of experiments were performed using a 157.5 mm long precision-bored glass tube with inner radius 31.5 ± 0.025mm (aspect ratio ≈ 5). The ends of the tube were sealed using machined aluminium caps with rubber 'O' ring seals. One cap had two 2mm threaded holes drilled through which enabled filling and removal of air bubbles. Once all

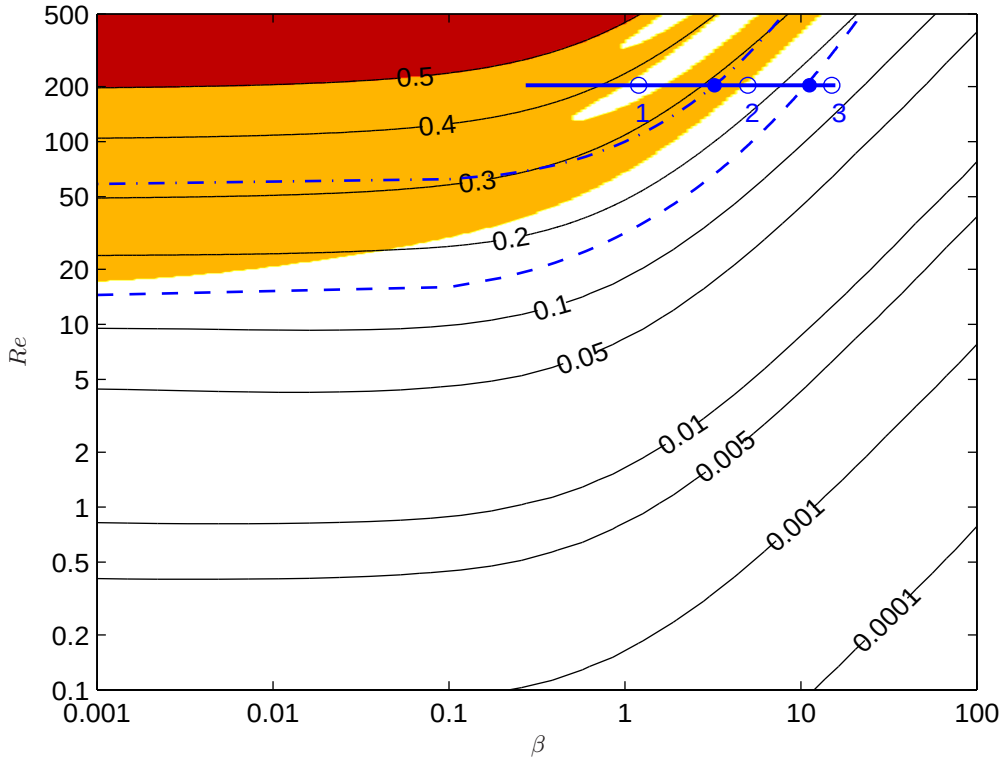

FIGURE 2. Contour plot of the maximum growth rate for $\alpha = 0.891$, $H/R = 5$ and $T = 0$. The lighter (orange) shaded area identifies the region where the maximum growth rate corresponds to λ_0 and the white region is where it corresponds to λ_1. The darker (red) shaded area indicates the region where the lengthscales of the instability are so small as to make any comparison between the axisymmetric and side-by-side flows practically meaningless: see figure 3. The region above the blue dashed (dash-dotted) line shows where the axisymmetric (asymmetric) instability no longer selects the fundamental axisymmetric (asymmetric) mode. The thick horizontal blue line and the blue circles which lie on it are used to illustrate features of the solution outlined in figure 4.

air was removed, the holes were sealed using nylon screws. Another set of experiments were carried out using a 32.0 ± 0.05mm machined acrylic tube which was 420 mm long (aspect ratio ≈ 13.1). The ends of this tube were sealed using similar machined aluminium end caps with 'O' ring seals but here the ends were held using 2mm steel rods which ran externally along the cylinder.

Experiments were performed by filling the cylinder 50:50 with the chosen fluids in a stable configuration with light over heavy fluid. It typically took approximately one week to allow all the air bubbles from the very viscous fluids to escape. The experiment was initiated by inverting the tube rapidly and the motion started typically ≈ 2 seconds after inversion. This initiation process was different to that used by Beckett et al. (2011) who removed a bung or slid a lid between the two reservoirs of viscous fluid. They report that this action typically took < 10 secs. In our experiments the motion was recorded using a high resolution Nikon D2XS digital camera operating in continuous mode at 8 frames

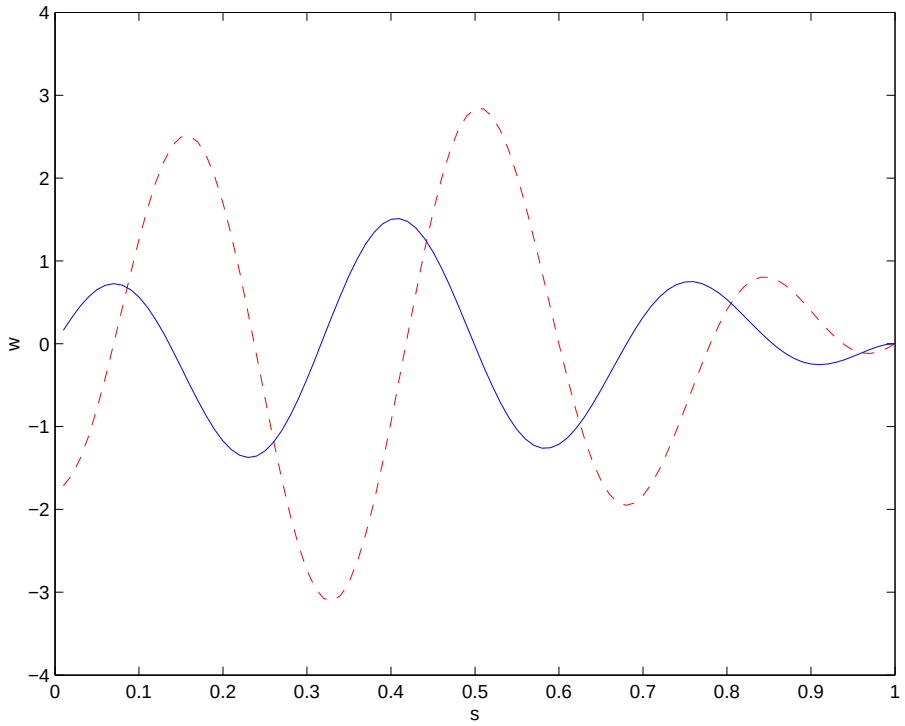

FIGURE 3. The λ_0 (dashed red) and λ_1 (solid blue) eigenfunctions for $(\alpha, H/R, T, \beta, Re) = (0.891, 5, 0, 0.1, 450)$ showing how the lengthscales of the preferred instability shorten in this part of parameter space.

per second. The image sequence was analysed using a Matlab script to edge-detect and thereby estimate the spatial location of the interface between the two fluids.

4. Stability Results

Specific representative values of α, H/R and T were chosen based upon the experiments performed in Beckett et al. (2011) and those done here. The ranges $\beta \in [0.001, 100]$ and $Re \in [0.1, 500]$ were treated to encompass the experimental ranges of Huppert & Hallworth (2007) and Beckett et al. (2011). Table 1 lists the various permutations used of α, H/R and T to examine their effects on which is the preferred instability. For all the parameters studied here $\lambda_2 < \lambda_1$ (noting the definition (2.19)) so that the focus below is on the competition between λ_0 (axisymmetric instability) and λ_1 (asymmetric instability).

Figure 2 shows the stability results for $\alpha = 0.891$, $H/R = 5$ and $T = 0$. The white region (low Re and high β) is where $\lambda_1 > \lambda_0$ so an asymmetric ($m = 1$) instability is preferred and the light orange region (high Re and low β) is where $\lambda_0 > \lambda_1$ so an axisymmetric instability is preferred. In the dark red upper region (essentially $Re \geqslant 200$ and $\beta \leqslant 1$), the instability becomes largely independent of the confining geometry (more than 5 nodes in the eigenfunction across the radius): see Fig 3 which shows typical eigenfunctions there which possess many spatial oscillations across the cylinder radius. The dash-dotted (dashed) line indicates where the fundamental asymmetric 'side-by-side' (axisymmetric 'core-annular') instability gives way to a higher wavenumber mode. This change in wavenumber is illustrated in figure 4 which focusses in on unexpected

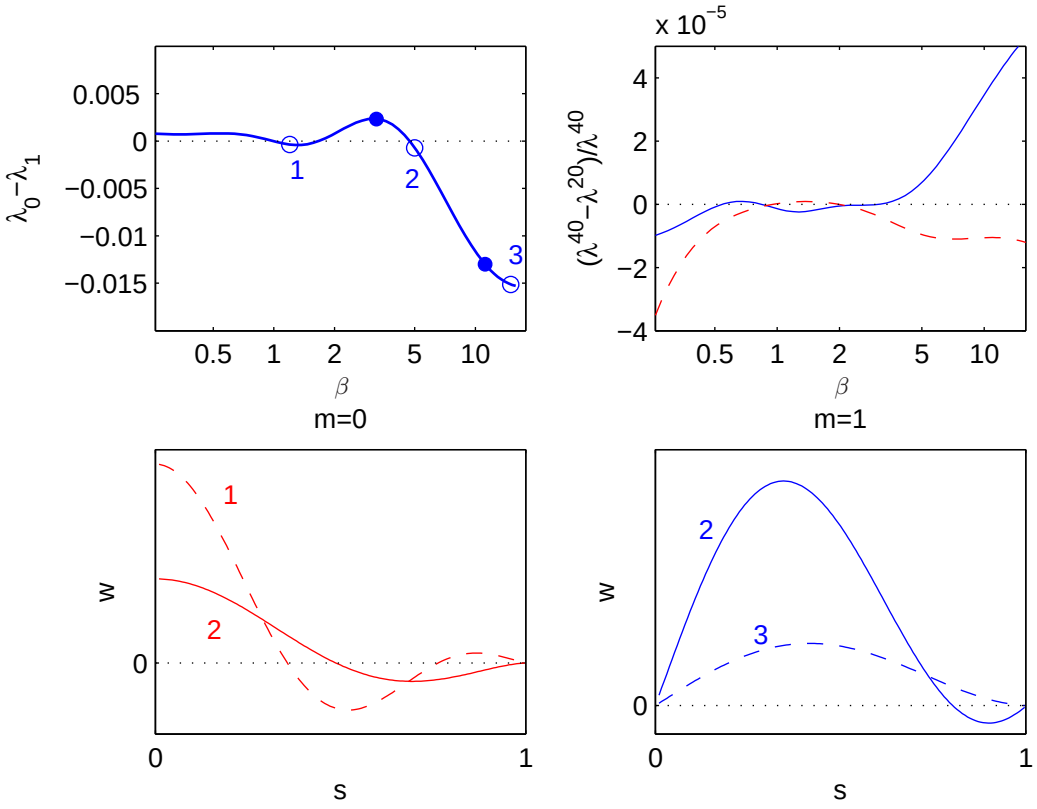

FIGURE 4. Plot (a) shows $\lambda_0 - \lambda_1$ over the range of β covered by the thick solid blue line in figure 2 confirming the existence of the $m = 1$ finger region in the area where the $m = 0$ mode dominates. The filled blue circles indicate where the fundamental mode at a given m is no longer preferred. Plot (b) demonstrates convergence: λ^{40} is the result using $(L, N) = (40, 40)$ and λ^{20} using $(L, N) = (20, 20)$ (blue solid $m = 1$, red dashed $m = 0$). Plots (c) and (d) show the $m = 0$ eigenfunctions at points 1 (red dashed),2 (red solid) and the $m = 1$ eigenfunctions at 2 (blue solid), 3 (blue dashed) respectively (all marked as open blue circles in figure 2). Note that between each pair of points an extra node is added to the fundamental eigenfunction.

islands (near $\beta \approx 1$ and $Re \approx 200$) where the two types of instability swap dominance. The (absolute) difference in the eigenvalues is $O(10^{-3})$ where both are ≈ 0.35 over this region (see their variation in figure 4 across the thick solid blue line drawn in figure 2) with the eigenvalues calculated down to a fractional accuracy of $O(10^{-5})$ (estimated by doubling the numerical resolution: see figure 4). Solid blue circles are drawn to indicate where the dashed and dash-dotted lines cross the solid blue line. Leading axisymmetric eigenfunctions are plotted at points 1 and 2 on this line (which straddle the dashed line) to indicate how an extra node (zero) in the eigenfunction exists at 1 compared to the fundamental eigenfunction at 2 which just has 1 node. Similarly, the leading asymmetric eigenfunctions are plotted at points 2 and 3 (which straddle the dash-dotted line) to indicate a similar increase in nodes (now from 0 to 1) going from 3 (the fundamental) to 2. The border of the light orange shading is everywhere at higher Re and lower β than the dash-dotted line indicating that the axisymmetric instability only becomes preferred once the asymmetric fundamental (side-by-side) instability is replaced by another asymmetric instability of smaller lengthscale.

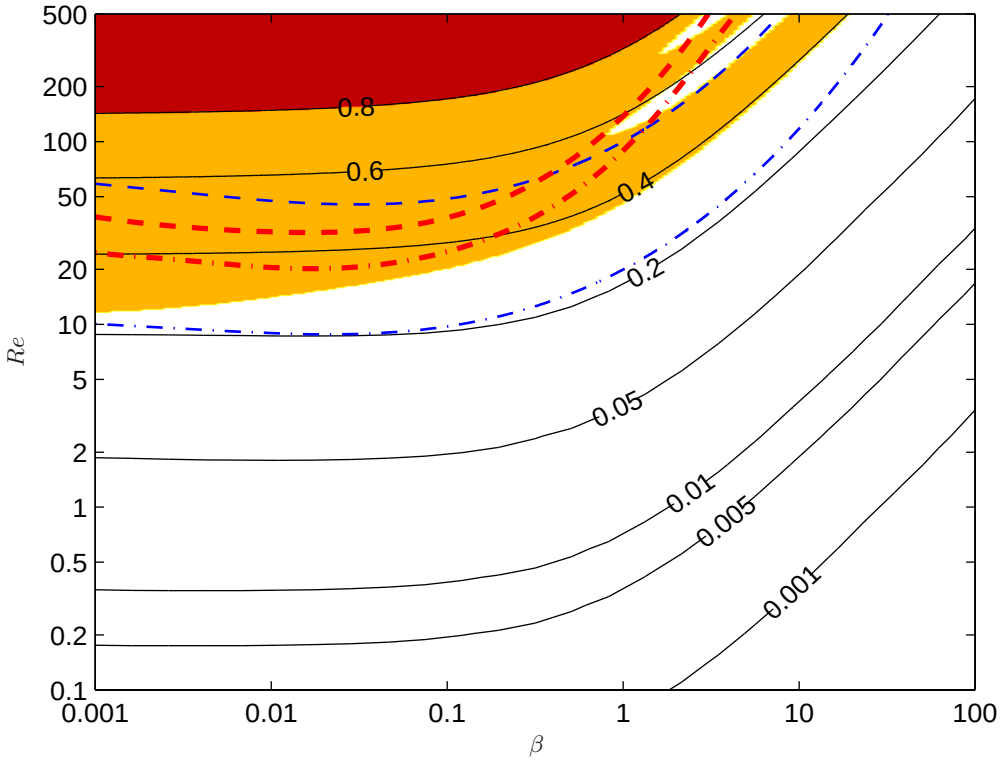

FIGURE 5. Contour plot of the maximum growth rate, λ, for $\alpha = 0.75$, $T = 0$, $H/R = 5$. As in figure 2 the dark (red) region indicates where the lengthscales are small, the light (orange) region where $\lambda_0 > \lambda_1$ and the white region where $\lambda_1 > \lambda_0$. (The shaded regions and lines represent the same quantities as in figure 2). The thick red dashed and dashed-dotted lines represent the predictions for the thin blue dashed and dashed-dotted line from a classical planar analysis (Chandrasekhar 1961).

A larger density contrast of $\alpha = 0.75$ is considered in figure 5 and the growth rates are found to correspondingly increase. The region where the Rayleigh-Taylor instability should be axisymmetric also increases slightly, stretching to slightly lower Re but otherwise the results are very similar to those at $\alpha = 0.891$. In particular, there are again interesting islands where the preferred instability can vary for small changes in Re and β. We also plot two further (thick) lines which are predictions from the standard planar analysis as to when the Rayleigh-Taylor instability should start to become geometry-independent i.e. select its own lengthscale rather than that imposed by the geometry. Specifically, the optimal wavenumber k_{max} for instability is found from the planar analysis for the same parameter values and a thick dashed line drawn when $2\pi/k_{max} = 3/2R$ for $m = 0$ (the condition that 3/2 wavelengths fit across the diameter) and a thick dash-dotted line when $\pi/k_{max} = R$ for $m = 1$ (one wavelength across the diameter). However, these new thick lines are not particularly good at predicting the location of the thin (red) dashed and dash-dotted lines which indicate when the preferred eigenfunctions start to select their own wavelength.

A more compact cylinder is considered in figure 6 (upper left plot). Growth rates look unchanged but now the region where the Rayleigh-Taylor instability is axisymmetric is

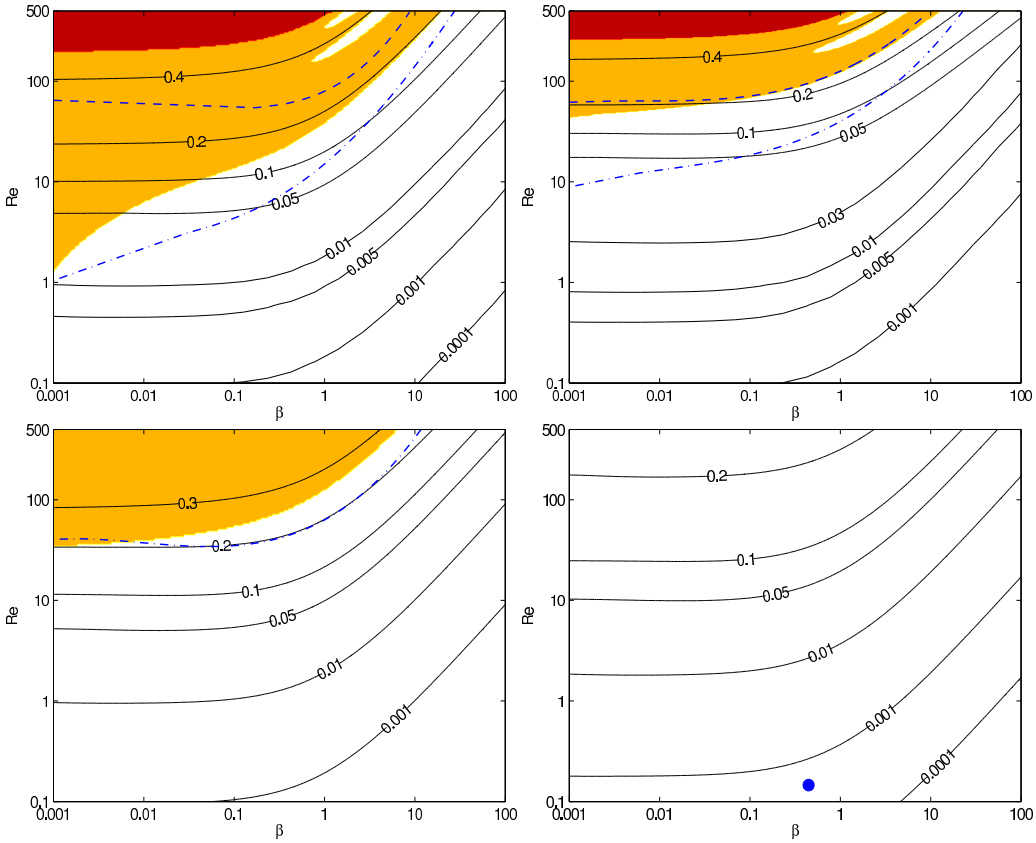

FIGURE 6. Contour plots of the maximum growth rate for (a) (upper left) $H/R = 2$, $\alpha = 0.891$, $T = 0$; (b) (upper right) $H/R = 10$, $\alpha = 0.891$, $T = 0$; (c) (lower left) $H/R = 5$, $\alpha = 0.891$, $T = 1 \times 10^{-3}$; (d) (lower right) $H/R = 5$, $\alpha = 0.891$, $T = 4 \times 10^{-3}$ (The shaded regions and blue lines represent the same quantities as in figure 2). Plot (c) has no dashed line so the preferred $m = 0$ instability is always the fundamental mode for the parameters shown. Plot (d) has no dashed or dash-dotted lines so both the $m = 0$ and $m = 1$ modes are geometry-dependent and it is the asymmetric, $m = 1$ mode which dominates over this range of Re and β. The blue dot in plot (d) denotes the point at which the eigenfunctions are plotted in figure 7.

noticeably lower at low β. For example, an axisymmetric instability can be expected for $Re \approx 2$ at $H/R = 2$ rather than at $Re \approx 20$ for $\beta = 0.001$. Again the change-over between axisymmetric and asymmetric instabilities happens beyond (higher Re and lower β) when the asymmetric instability is no longer the fundamental side-by-side instability. For a taller cylinder - upper right plot in figure 6 - growth rates decrease and the region of preferred axisymmetric Rayleigh-Taylor instability recedes. Now in the region where the axisymmetric instability is preferred, the instability is not generally the fundamental mode except for small part of the (β, Re) plane given by $\beta < 0.1$ and $Re \approx 50$. The lower plots in figure 6 explore the effect of introducing surface tension between the two fluids. Comparing the results with figure 2, one can see a trend of decreasing growth rates as T increases and the recession of the preferred axisymmetric instability region to higher Re and lower β. By $T = 4 \times 10^{-3}$, which is the non-dimensional value of the surface tension between golden syrup and silicone oil ($\approx 60 \times 10^{-3}$N/m using $\rho_1 = 1.5 g/cm^3$ and $R = 3.2cm$), only an asymmetric side-by-side instability is ever predicted. Figure 7 shows the leading axisymmetric and asymmetric eignefunctions for a typical set of experimental

parameters which both (not surprisingly) emphasize the localisation of the initial vertical flow at the interface.

4.1. *Comparison with available observations.*

In their figure 5, Beckett et al. (2011) indicate the structure of a six starting flows (experiments 6, 11, 12, 15, 19 and 22) at short distances from the initial interface (the interface at $t = 0$ is obscured by an opaque release collar). These experiments have $0.9 < \alpha < 1$, $5 < \beta \leqslant 375$, $Re < 0.31$ as well as $T = 0$ and H/R effectively infinite. The upper right plot in figure 6 is therefore most appropriate and this unambiguously predicts a side-by-side (fundamental asymmetric) Rayleigh-Taylor instability. This is consistent with 5 of these 6 experiments. The one exception is experiment 6 which shows an initial axisymmetric Rayleigh-Taylor instability which then develops over time into a side-by-side flow. Contrarily, experiments 11 and 15 show initial side-by-side instabilities which later develop into axisymmetric core-annular flows. These results generally confirm the linear stability analysis but also indicate that the initial instability is *not* a reliable indicator of the late-time flow configuration. This latter conclusion is also supported by the experiment in figure 1 where the initial instability is side-by-side but the later time flow is predominantly axisymmetric.

The focus of Stevenson & Blake's (1998) study was the long-time exchange flow but the sketches in their figure 2 suggest an asymmetric instability for $\beta \gtrsim 0.1$ (their $\mu_d/\mu_c = 1/\beta$) and an axisymmetric instability otherwise for their parameters of $0.70 \leqslant \alpha \leqslant 0.94$ and $0.01 \leqslant Re \leqslant 12$. This is loosely consistent with the theoretical results presented in figure 5 (the most appropriate figure as their fluids were miscible, the geometry was large aspect ratio $H/R = 100$ and $\alpha \approx 0.70$ for some of their apparent axisymmetric instabilities). The theoretical stability results in figure 5 show a fastest growing asymmetric instability for $\beta > 0.1$ and $Re \leqslant 12$ which is consistent with their experiments and the possibility of a fastest growing axisymmetric instability for $\beta \lesssim 10^{-3}$ and $Re \lesssim 12$. Extrapolating this region back to even lower values of β would suggest a preferred axisymmetric instability at $Re = O(1)$ when $\beta = O(10^{-5})$. The experiments satisfying their criterion $\mu_d/\mu_c \gtrsim 300$ presumably display an unequivocal axisymmetric instability (experiments 2 and 5-8 relisted in Table 2 using the current non-dimensional parameters) and are at least close to, if not precisely in, this region. Stevenson & Blake (1998) also observed that the long-time flow didn't necessarily follow the form of the initial instability with the less dense fluid always rising up the centre regardless of the initial instability.

Accessing the axisymmetric instability regime is, however, difficult and our attempts with immiscible fluids of low viscosity (silicone oil and pure alcohol) failed due to two issues with the experimental set-up. Firstly, the small interfacial tension required meant that the fluids tended to mix at the interface which is not accounted for in the theory. Secondly, the action of the initial inversion of the tube produced asymmetric inertial motion which favoured the side-by-side instability (this was not an issue for the more viscous fluids used elsewhere in the study as there was no correlation between the sense of the asymmetric instability and the inversion direction). Both difficulties (which didn't apparently bother Stevenson & Blake 1998), however, could potentially be avoided using a different experimental protocol in which the fluids are arranged stably and then accelerated downwards faster than gravity to recreate unstable conditions as in the work of Jacobs and coworkers (Jacobs et al. 1985, Jacobs & Catton 1988 and Wilkinson & Jacobs 2007).

Experiment	α	β	Re	$v/(\frac{1}{2}\Delta\rho g R^2/\mu_2)$	U^+
1	0.95	1.5×10^{-2}	0.27	1.9×10^{-3}	0.011
2	0.80	5.4×10^{-5}	0.10	7.0×10^{-3}	9×10^{-4}
3	0.91	0.79	5.34	0.036	0.045
4	0.90	0.43	2.55	0.028	0.033
5	0.80	5.9×10^{-4}	5.33	7.2×10^{-5}	2.8×10^{-3}
6	0.90	7.3×10^{-4}	0.17	9.8×10^{-5}	3.1×10^{-3}
7	0.70	2.9×10^{-5}	0.71	3.8×10^{-6}	6.6×10^{-4}
8	0.70	3.3×10^{-5}	0.81	4.1×10^{-6}	7.0×10^{-4}
9	0.88	3.4×10^{-2}	0.50	4.1×10^{-3}	0.014
10	0.91	0.47	11.79	0.034	0.016
11	0.91	0.47	4.88	0.030	0.016

TABLE 2. Data from Table 2 in Stevenson & Blake (1998) translated into the current non-dimensional parameters. Throughout $H/R = 100$ and $T \approx 0$. Experiments 3,4,10 & 11 apparently show asymmetric initial instabilities and experiments 2, 5-8 axisymmetric initial instabilities. The 2nd column from the right, $v/(\frac{1}{2}\Delta\rho g R^2/\mu_2)$, is the non-dimensionalised speed measured by Stevenson & Blake (1998) for the upward moving finger in their experiments. The rightmost column is the corresponding prediction from section 5.

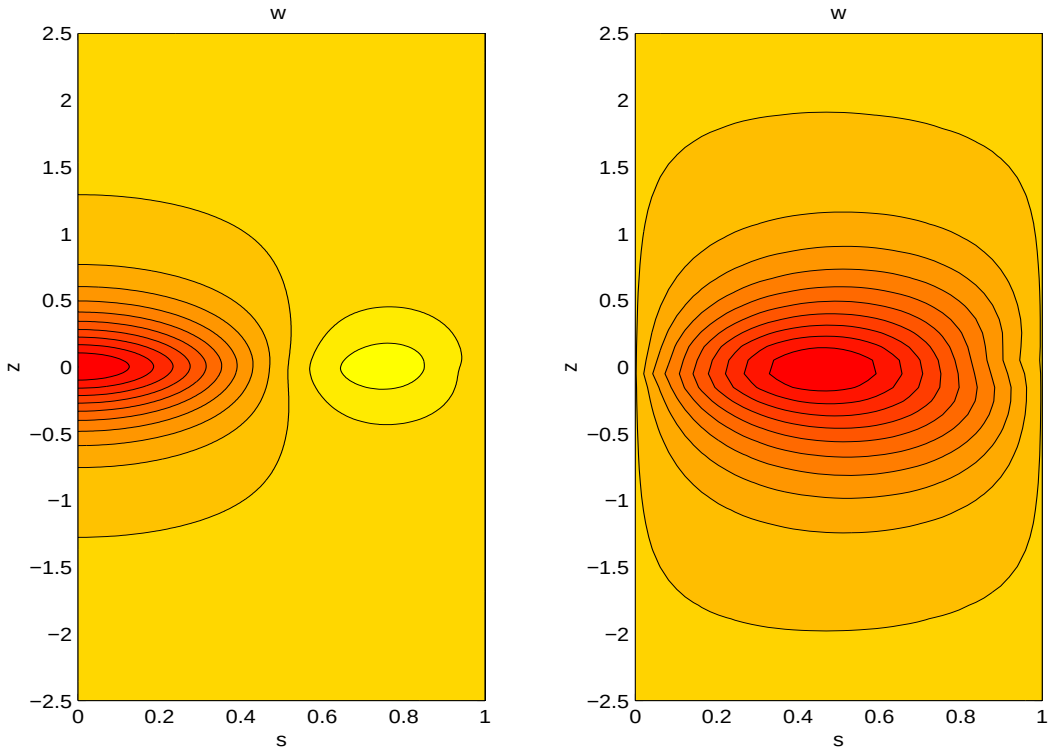

FIGURE 7. Plots of the w component of the most unstable eigenfunctions for $m = 0$ (left) and $m = 1$ (right) at $\beta = 0.445$, $Re = 0.149$, $\alpha = 0.891$, $T = 4\times10^{-3}$ and $H/R = 5$ - a typical experimental set-up and are marked as a blue dot on the lower right plot in figure 6. (The velocities are normalised to have a maximum speed of 1 and contour levels are from -1.01 to 0.2 in steps of 0.1. The shading near the walls represents 0.)

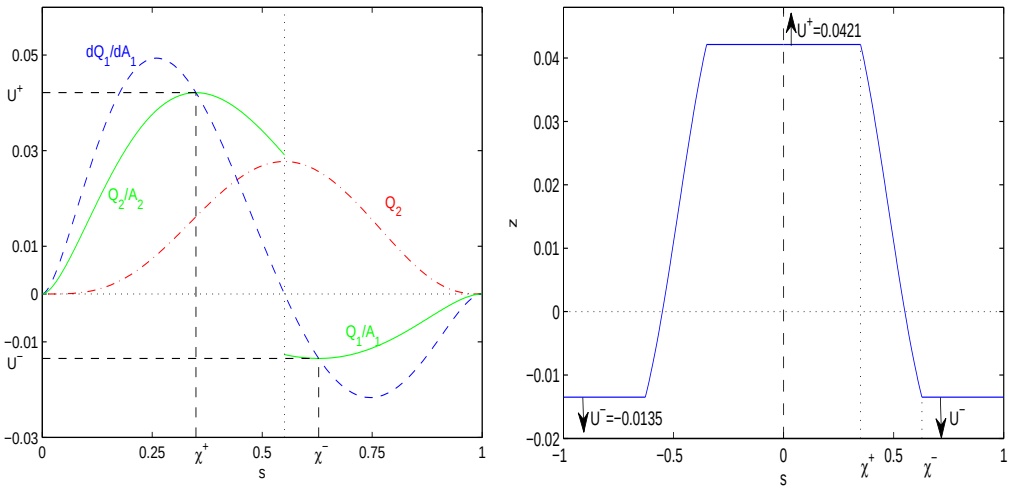

FIGURE 8. (a) The characteristic speed dQ_i/dA_i (dashed blue line) as a function of the radius for $\beta = 2$. Shocks need to be fitted when $dQ_i/dA_i = Q_i/A_i$ the latter shown in solid green lines for $i = 1, 2$. (b) shows the corresponding solution at $t = 1$ with shocks fitted (for later times, just rescale the z-axis as the speeds are constant in time).

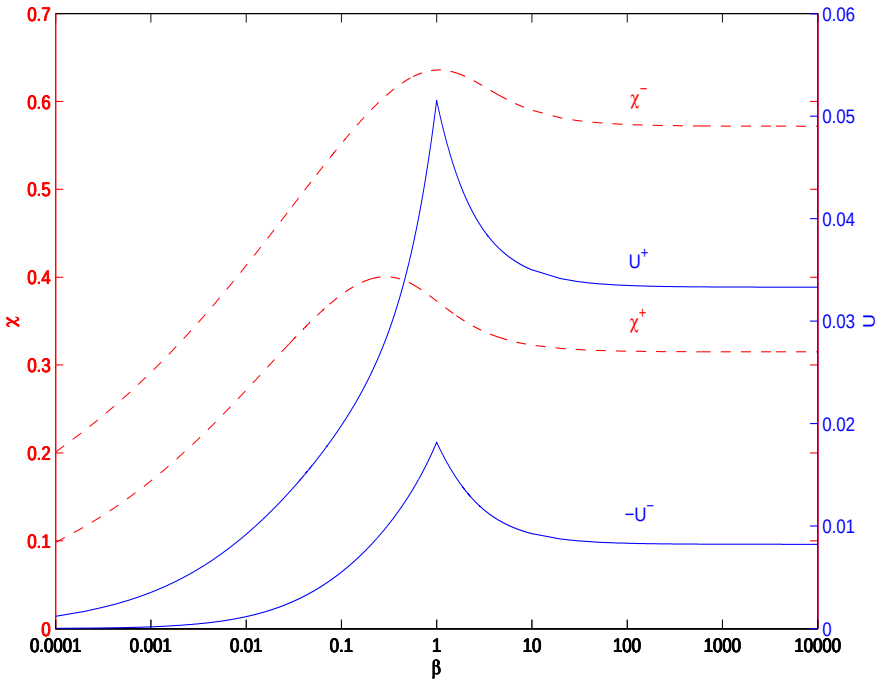

FIGURE 9. Variation of the shock velocities $U^{\pm}$ and shock positions $\chi^{\pm}$ with viscosity ratio β. The cusp in the velocities at $\beta = 1$ is the result of a change in non-dimensionalisation which is always done using the viscosity of the less viscous fluid as in K11) ($U^{\pm} \to \beta U^{\pm}$ for $\beta < 1$).

5. Long Time Fingering Solutions

So far, we have been concerned with predicting the form of the preferred initial linear instability for a given set of parameters. Here, we focus on constructing plausible long-time fingering solutions based upon the assumption that the fluid-fluid interface varies slowly along the cylinder compared to across it. This is not strictly true at the end of the finger but it is still of interest to see if this appealing approximation proves useful in predicting the propagation speed of the finger. This approach is natural *if* the form of the initial linear instability dictates the long time form of the nonlinear finger solution (e.g. a core-annular instability develops into a long core-annular finger) but is still useful even if this is not always so as experiments indicate (see figure 1b & c, figure 5 in Beckett et al. 2011, and Stevenson & Blake 1998). Then the idea is that if a finger of a given form is observed, a prediction can be made for its speed regardless of what the initial instability was.

The analysis proceeds by adding slow axial variation to the axially-independent solutions described in Huppert & Hallworth (2007) and Kerswell (2011, hereafter K11). If $\partial/\partial z = O(\epsilon|\nabla_h|)$ where $\epsilon \ll 1$ and ∇_h is the horizontal gradient, then to leading order the equations describing the motion of the two fluids are just (reinserting dimensions for a moment indicated by $*$)

$$-G(z) = \mu_1 \nabla_h^2 w_1^* - \rho_1 g \quad \text{in} \quad A_1^*, \qquad -G(z) = \mu_2 \nabla_h^2 w_2^* - \rho_2 g \quad \text{in} \quad A_2^* \tag{5.1}$$

(where fluid i occupies the domain $A_i^*(z,t)$, $G(z,t)$ is the slowly varying pressure gradient and $\nabla_h^2 := \nabla^2 - \partial^2/\partial z^2$ is the horizontal Laplacian) together with mass conservation

$$\nabla_h \cdot \mathbf{u}_i^{*h} + \frac{\partial w_i^*}{\partial z} = 0 \qquad i = 1, 2 \tag{5.2}$$

where $\mathbf{u}_i^{*h}$ is the $O(\epsilon)$ horizontal (cross-sectional) velocity of fluid i. These are to be solved subject to non-slip boundary conditions at the tube wall and continuity of velocity and stress at the interface Γ between the two fluids, that is

$$w_1^* = w_2^* \quad \& \quad \mu_1 \frac{\partial w_1^*}{\partial n} = \mu_2 \frac{\partial w_2^*}{\partial n} \quad \text{on} \quad \Gamma \tag{5.3}$$

(where $\partial/\partial n$ is the normal derivative to Γ) together with the condition of no net volume flux at any one cylindrical height

$$\int w_1^* \, dA_1^* + \int w_2^* \, dA_2^* = 0. \tag{5.4}$$

As in K11 and in contrast to the previous sections 2-4, the system is non-dimensionalised using the tube radius R, the differential hydrostatic pressure gradient $\Delta\rho g$ (where $\Delta\rho := \rho_1 - \rho_2$) and μ_1 so that after defining λ by

$$G(z,t) = \tfrac{1}{2}(\rho_1 + \rho_2)g - \tfrac{1}{2}\Delta\rho g \lambda(z,t) \tag{5.5}$$

then

$$\nabla_h^2 w_1 = \lambda + 1 \quad \text{in} \quad A_1, \tag{5.6}$$

$$\beta \nabla_h^2 w_2 = \lambda - 1 \quad \text{in} \quad A_2, \tag{5.7}$$

$$w_1 = w_2 \quad \& \quad \frac{\partial w_1}{\partial n} = \beta \frac{\partial w_2}{\partial n} \quad \text{on} \quad \Gamma \tag{5.8}$$

where, compared to eqns (2.4)-(2.7) of K11), there are the further equations

$$\nabla_h \cdot \mathbf{u}_i^h + \frac{\partial w_i}{\partial z} = 0 \qquad i = 1, 2. \tag{5.9}$$

(Henceforth w_1 and w_2 are in units of $\frac{1}{2}\Delta\rho g R^2/\mu_1$ and the one-fluid volume fluxes

$$Q_i := \int w_i \, dA_i \qquad i = 1, 2 \tag{5.10}$$

are in units of $\frac{1}{2}\Delta\rho g R^4/\mu_1$ with $A_1 \cup A_2$ being the unit disk.) The horizontal velocities can be eliminated by integrating either one of the mass conservation equations over an elemental volume made up of two nearby horizontal cross-sections to give

$$\frac{\partial A_i}{\partial t} + \frac{\partial Q_i}{\partial z} = 0 \qquad i = 1, 2. \tag{5.11}$$

Now, providing A_i is parametrised by one variable, $\chi(z,t)$, these latter equations can be rewritten as one equation

$$\frac{\partial \chi}{\partial t} + \frac{dQ_i}{dA_i}\frac{\partial \chi}{dz} = 0 \tag{5.12}$$

(since $Q_1 + Q_2 = 0$ and $A_1 + A_2 = \pi$, $dQ_1/dA_1 = dQ_2/dA_2$) which a 1st order hyperbolic PDE for χ. Without loss of generality, χ can be defined such that $A_2 \to 0$ as $\chi \to 0$ and $A_1 \to 0$ as $\chi \to 1$. In this case, a fingering solution consists of χ decreasing monotonically from 1 (entirely fluid 2) to 0 (entirely fluid 1) across a long but finite length of the cylinder as height increases. A straightforward way of generating such a solution is to solve the Riemann problem where at $t = 0$

$$\chi(z, 0) = \begin{cases} 0 & z > 0, \\ 1 & z < 0. \end{cases} \tag{5.13}$$

This procedure is best illustrated in the simplest case of an axisymmetric fingering solution (the more complicated 'side-by-side' fingering solution is discussed in Appendix C). Here χ is most sensibly chosen as the radius of the circular interface between the two fluids with the lighter fluid rising up the core ($A_1 = \pi(1-\chi^2)$ and $A_2 = \pi\chi^2$). In this case the flow fields can be written down explicitly (K11, eqns (2.12) & (2.13)) as

$$w_1 = \frac{\lambda+1}{4}(s^2 - 1) - \chi^2 \log s \qquad \chi \leqslant s \leqslant 1, \tag{5.14}$$

$$w_2 = \frac{\lambda-1}{4\beta}(s^2 - \chi^2) - \chi^2 \log \chi - \frac{\lambda+1}{4}(1-\chi^2) \qquad s \leqslant \chi. \tag{5.15}$$

The corresponding flux functions are

$$Q_1 = \frac{\pi}{8}[(\lambda+1)(2\chi^2 - \chi^4 - 1) + 4\chi^2(1-\chi^2) + 8\chi^4 \log \chi], \tag{5.16}$$

$$Q_2 = \frac{\pi}{8\beta}[(1-\lambda)\chi^4 - 2\beta(1+\lambda)\chi^2(1-\chi^2) - 8\beta\chi^4 \log \chi], \tag{5.17}$$

with the net flux constraint $Q_1 + Q_2 = 0$ requiring the pressure gradient to be

$$\lambda = \frac{(3\beta - 1)\chi^4 - 4\beta\chi^2 + \beta}{(\beta - 1)\chi^4 - \beta}. \tag{5.18}$$

The hyperbolic equation (5.12) has characteristics $z = Z(t)$ where

$$\frac{dZ}{dt} = \frac{dQ_i}{dA_i} = \frac{dQ_i/d\chi}{dA_i/d\chi} \tag{5.19}$$

along which χ is constant. Hence the characteristics are straight lines in the (z,t) plane. For the Riemann problem, they all emanate from $z = 0$ at $t = 0$ in what would be a rarefaction fan *if* the characteristic speed is a monotonically decreasing function of χ.

However, this is not the case as generically $dQ_i/dA_i \to 0$ for $\chi \to 0$ or 1. Figure 8, which takes $\beta = 2$, shows the typical behaviour of dQ_i/dA_i as a function of the radius s. The regions of positive d^2Q_i/dA_i^2 are near the limiting values of χ so two shocks need to be fitted to avoid the clashing of characteristics (note again as $Q_1+Q_2 = 0$ and $A_1+A_2 = \pi$, $d^2Q_1/dA_1^2 = d^2Q_2/dA_2^2$). By considering mass conservation, a shock must be fitted to move at the speed

$$U := \frac{[Q_i]^+_-}{[A_i]^+_-} \tag{5.20}$$

where $[\quad]^+_-$ indicates the jump across the shock and $i = 1$ or 2. The only consistent way to fit two such shocks into the rarefaction fan is to have the rest state $\chi = 0$ above the upward-propagating shock and the rest state $\chi = 1$ below the downward-propagating shock. Then the two shocks each have to follow a characteristic which means

$$U = \frac{dQ_i}{dA_i}|_{\chi^*} \qquad \text{where} \quad \frac{dQ_i}{dA_i}|_{\chi^*} = \frac{Q_i}{A_i}|_{\chi^*} \tag{5.21}$$

with two solutions for χ^* near 0 (defined as $s = \chi^+$ where $U = U^+$) and near 1 (defined as $s = \chi^-$ where $U = U^-$) giving the shock radii. Both shocks therefore move with constant speed. Figure 8 shows that for $\beta = 2$, $U^+ = 0.0421$ (the speed of the upward propagating finger) with χ^+ outside of the maximum of dQ_i/dA_i and $U^- = -0.0135$ (the speed of the downward propagating ring of fluid) for χ^- inside of the minimum of dQ_i/dA_i (the radial positions of this maximum and minimum act as lower and upper limits respectively on the shock positions). Figure 8 also shows the corresponding flow solution at $t = 1$ (since the shocks move at constant speed the solution looks exactly the same for all times albeit with the $z-$axis rescaled appropriately). Figure 9 indicates how these predicted speeds and shock locations vary with the viscosity ratio β. The cusps in $U^\pm$ centred at $\beta = 1$ are the result of a rescaling for $\beta < 1$ so that the dynamic viscosity used in the non-dimensionalisation is always the smaller of the two fluids (as in K11). Hence for $\beta < 1$, μ_1 is replaced by μ_2 which means that $U^\pm$ in units of $\frac{1}{2}\Delta\rho g R^2/\mu_1$ is $\beta U^\pm$ in units of $\frac{1}{2}\Delta\rho g R^2/\mu_2$. The fact that the shock speeds tend to zero for $\beta \to 0$ is a reflection of the fact that the more viscous fluid struggles to descend against the tube walls. The figure also shows that shocks must always be fitted across a significant part of the flow domain ($[0, \chi^+] \cup [\chi^-, 1]$) for this type of fingering solution. Given this, it is unclear how good an estimator the required shock speeds are for the the true fingering speeds. One would hope that they are if the main bulk (interior) of the exchange flow solution determines the finger motion as it seems to in horizontal exchange flows (e.g. Matson & Hogg 2012).

5.1. *Fingering states: experimental results*

In both the experiments of Stevenson & Blake (1998) and Beckett et al. (2011), miscible fluids were used in the experiments (e.g. pure golden syrup was positioned above a water-diluted golden syrup). Long slowly moving fingers were observed by both teams but speeds were only reported for the upward-propagating finger in Stevenson & Blake (1998). A comparison of their measurements with the theoretical predictions (figure 9) is not good: see the last two columns in Table 2. The predicted speed is comparable although not accurate for $\beta = O(1)$ but is more than an order of magnitude out if the two fluids have very different dynamic viscosities ($\beta \lesssim 10^{-3}$).

To explore the reasons for this discrepancy further, we performed some experiments of our own. Golden syrup and $600cm^2/s$ silicone oil were chosen for a batch of 8 runs (each taking a week!) using either the short or the long cylinders. All revealed an initial

constant acceleration for the first 1.5 to 2 seconds after which both interfaces travelled at a constant speed: see figure 10. The speed remained constant until the interface reached $\sim 95\%$ of the length of the cylinder. At this point the presence of the end wall was felt and the motion of the interface slowed. The estimates for the speed of propagation were repeatable to within $\sim 4\%$ between runs of the experiment and those performed in the short tube were typically $\sim 14\%$ smaller than those found in the long tube.

The evolution of the interfaces for one particular experiment ($\beta = 0.445$) in the long tube are plotted in figure 10: the downward-moving interface has a speed of $6.27 \pm 0.25\text{mms}^{-1}$ and the upward-moving interface a speed of $10.84 \pm 0.4\text{mms}^{-1}$. The theoretical predictions of 0.5mms^{-1} and 1.4mms^{-1} (respectively) are again poor consistent with the comparisons in Table 2. Observations of the realised flow revealed it to be far from being two oppositely moving slowly-varying fingers each with a small head. Instead, each finger developed a very blunt, almost bulbous, nose instead: see figure 10. The fact that the interfaces have already reached a constant, apparently terminal, speed is highly suggestive that figure 10 is in the asymptotic state (note only the central $\approx 5R$ of the $13.1R$ long cylinder is shown in figure 10). The initial instability was asymmetric but quickly evolved to become increasingly axisymmetric with the upward-moving and downward-moving fluid both migrating towards the centre of the cylinder: see figures 1 and 10 which are consistent with the sketch in figure 2(a) of Stevenson & Blake (1998). An apparent consequence of this migration is the interesting development of a cusp at the initial position of the interface. The cusp forms on the centreline at $z = 0$ approximately 2 seconds after the overturn, contains dense fluid and is advected upwards by the upward-moving, less-dense fluid. The cusp stays central as it progresses upwards at 13.5mms^{-1}, that is, about a third faster than the upward-moving interface so that it eventually catches up with it.

Since the interface speeds quickly reach their terminal values well before the cusp travels very far, the most plausible explanation for the poor theoretical prediction is the failure to model the the fluid dynamics at the finger ends properly. The theoretical assumption of slow axial variation is always violated at the finger ends and so the true fluid dynamics cannot be captured in this approximation. Nevertheless, the *a priori* hope is that this end region is actually not important compared to the dynamics of the bulk of the finger (as, for example, in the horizontal exchange problem, Matson & Hogg 2012). It now seems that this is a vain hope in the vertical exchange problem. The existence of the cusp is an unexpected and intriguing observation which issues a significant challenge to direct numerical simulations of the Navier-Stokes equations.

6. Discussion

In this study we have considered the Rayleigh-Taylor linear instability problem for two viscous and immiscible fluids in the situation when each half-fill a finite cylinder aligned with gravity. This problem depends on a formidable 5 parameters but a good feel for how the preferred instability varies in structure is possible by sampling a few representative values for the density difference, the surface tension and the geometry while sweeping continuously across the viscosity ratio and Reynolds number. Focussing on the parameter regime where the instability wavelength is comparable with the cylinder radius, we find that the preferred instability is predominantly asymmetric with azimuthal wavenumber 1 indicating a 'side-by-side' initial flow. This is then consistent with findings in the continuously stratified situation (Wooding 1959, Batchelor & Nitsche 1993) and the miscible problem (Vanaparthy et al. 2003, 2008). There is, however, a region of parameter space (high Re and low β) where the preferred instability is axisymmetric for

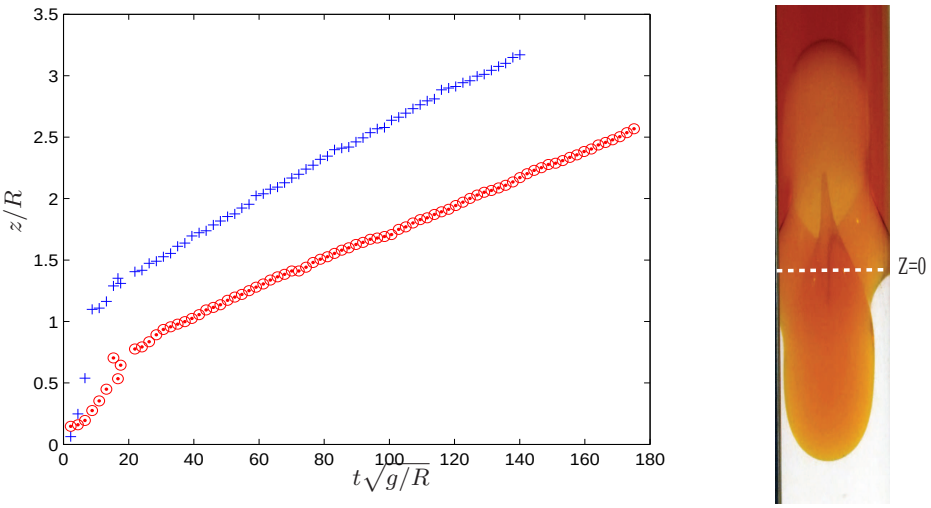

FIGURE 10. Left: a plot of the (non-dimensionalised) distance z/R versus time for the downward (red lower circles) and upward (blue upper +) traveling interfaces measured from experiments using golden syrup and 600cm^2/s silicone oil ($\beta = 0.445$) in the 42cm tube ($R = 3.2$cm). Right: frontview of a cusp formed ~ 6 seconds or $t\sqrt{g/R} \sim 105$ after the start of the experiment by which time the upward-moving interface has travelled $\approx 2.5R$ up the cylinder.

which there is anecdotal evidence (Stevenson & Blake 1998) but which is difficult to verify experimentally at least with the 'inversion' strategy. This region recedes to higher Re and lower β with increasing surface tension until at $T = 4 \times 10^{-3}$, the preferred instability is always asymmetric for $\alpha = 0.891$, $H/R = 5$ and $(\beta, Re) \in [0.001, 100] \times [0.1, 500]$ (see figure 6).

Slow fingering solutions have also been constructed by adding slow axial variation to the 2-dimensional exchange solutions recently described in K11. These represent plausible approximations to observed long-time Rayleigh-Taylor flows (Stevenson & Blake 1998, Beckett et al. 2011) and make predictions for the speed of the fingers. The fact that the predictions turn out to be poor indicates that, in contrast to the horizontal exchange flow problem (Matson & Hogg 2012), the fluid dynamics at the ends of the fingers is *not* subservient to that in the slowly-varying bulk. Experiments have also revealed an interesting cusp formation at the interface which indicates that the ensuing exchange flow has a more complicated structure than previously thought.

In terms of the original motivation, we find very good (although not perfect) agreement between what the linear stability analysis predicts and what the flow actually looks like near to the initial interface as reported by Beckett et al. (2011) and inferred from Stevenson & Blake (1998). The fact that the long time flow can have a different axial symmetry to that of the original instability - highlighted in figures 1 and 10 - indicates that the initial Rayleigh-Taylor instability does *not* uniquely determine the form of the long-time flow configuration although it may well strongly influence it. Determining what does remains an outstanding question.

Acknowledgements. This work represents the Master's thesis of Helen Sweeney who thanks EPSRC for their support. TM is grateful to Finn Box for help with the Matlab script used for edge detection.

Appendix A: Numerical Method

The partial differential eigenvalue problem is converted into an algebraic eigenvalue problem by using the following spectral expansions: for m even,

$$\begin{bmatrix} \bar{u}_i \\ \bar{v}_i \end{bmatrix} = \sum_{l=0}^{L-1}\sum_{n=0}^{N-1} \begin{bmatrix} u_i^{ln} \\ v_i^{ln} \end{bmatrix} \Theta_{2l+1}(s)T_{2n+1}(z_i), \tag{6.1}$$

$$\bar{w}_i = \sum_{l=0}^{L-1}\sum_{n=0}^{N-1} w_i^{ln}\Theta_{2l}(s)T_{2n+1}(z_i), \tag{6.2}$$

$$\bar{p}_i = \sum_{l=0}^{L-1}\sum_{n=0}^{N-1} p_i^{ln}T_{2l}(s)T_{2n}(z_i) \tag{6.3}$$

and for m odd,

$$\begin{bmatrix} \bar{u}_i \\ \bar{v}_i \end{bmatrix} = \sum_{l=0}^{L-1}\sum_{n=0}^{N-1} \begin{bmatrix} u_i^{ln} \\ v_i^{ln} \end{bmatrix} \Theta_{2l}(s)T_{2n+1}(z_i), \tag{6.4}$$

$$\bar{w}_i = \sum_{l=0}^{L-1}\sum_{n=0}^{N-1} w_i^{ln}\Theta_{2l+1}(s)T_{2n+1}(z_i), \tag{6.5}$$

$$\bar{p}_i = \sum_{l=0}^{L-1}\sum_{n=0}^{N-1} p_i^{ln}T_{2l+1}(s)T_{2n}(z_i). \tag{6.6}$$

with $i = \{1, 2\}$. Here

$$\Theta_l(s) := T_{l+2}(s) - T_l(s) \tag{6.7}$$

where $T_n(x) := \cos(n \cos^{-1} x)$ is the nth Chebyshev polynomial and

$$z_1 := 1 - \frac{2Rz}{H} \quad z \geqslant 0 \qquad \& \qquad z_2 := \frac{2Rz}{H} + 1 \quad z \leqslant 0. \tag{6.8}$$

(There is a small subtlety for $m = 0$ where as written above, the pressure expansions have a constant value in both the upper and lower domains. This degeneracy is removed by replacing p_2^{00} by an extra spectral term corresponding to the coefficient p_2^{0N}.) The non-slip boundary conditions are inbuilt into these expansions: for example, at $z = H/2R$, $z_1 = 0$ and $T_{2n+1}(0) = 0$ for all n, and $\Theta_l(1) = 0$ for all l. The correct parity of each variable with respect to s based upon whether m is even or odd (see the Appendix of Kerswell & Davey 1996) is also directly enforced which has two important consequences. Firstly, this avoids numerical problems at the coordinate singularity $s = 0$ by building in the correct behaviour there automatically. Secondly, a given truncation is twice as efficient in representing the solution as a generic spectral expansion retaining both parities. The various constraints specifying the expansion coefficients are imposed for $m \neq 0$ by collocating the equations and interface conditions as follows

	$s_1 \quad \cdots \quad s_L$	
z_1^1 $\vdots$ z_1^{N-1}	$\nabla.\mathbf{u}_1 = 0$ u_1, v_1, w_1 momentum eqs	4L(N-1) equations
z_1^N	w_1 momentum eq	L equations
$z_1^{N+1} = z_2^{N+1} = 0$	interface conditions	6L equations
$-z_2^N$	w_2 momentum eq	L equations
$-z_2^{N-1}$ $\vdots$ $-z_2^1$	$\nabla.\mathbf{u}_2 = 0$ u_2, v_2, w_2 momentum eqs	4L(N-1) equations

which gives $8LN$ equations for $8LN$ unknown coefficients. Here, s_j for $j = 1, \ldots, L$ are the L positive zeros of $T_{2L}(s)$ and z_1^j $(-z_2^j)$ are the N positive (negative) zeros of T_{2N} indexed such that the collocation points are clustered just above (below) the interface at $z_1^{N+1} = z_2^{N+1} = 0$. These choices ensure that areas where the eigenfunctions should be most challenging to resolve are sampled most efficiently. For $m = 0$, there is a simplification in that the azimuthal flow component decouples from the others and is, in fact, zero for the unstable eigenfunctions. This reduces the equation count down to $3L(N-1) + L + 4L + L + 3L(N-1) = 6LN$ in a straightforward way. In either case, the resulting generalised eigenvalue problem $Ax = \lambda Bx$ is then solved (using LAPACK routine DGGEV) to identify the important eigenvalues which are then efficiently traced around in parameter space using inverse iteration. Typical resolutions used were $(L, N) = (20, 20)$ for DGGEV which takes about 6 mins and $(L, N) = (30, 30)$ for inverse iteration which takes about 2 minutes (both on an Intel Xeon X5670).

Appendix B: Exact Solutions for a Rayleigh-Taylor problem with different boundary conditions

This appendix outlines the existence of simple exact viscous solutions of the Rayleigh-Taylor instability problem in an infinite cylinder for appropriately-modified tangential boundary conditions on the cylinder. This modified problem provides a valuable check on the full numerical code used in the main part of the paper. The Rayleigh-Taylor problem basically involves solving

$$\lambda \mathbf{u} + \nabla p = \frac{1}{Re} \nabla^2 \mathbf{u} \quad \& \quad \nabla \cdot \mathbf{u} = 0 \tag{6.1}$$

in two domains which are matched together. It is straightforward to show that there is the separable solution

$$
\begin{aligned}
w^+ &= \left(A_1^+ e^{ik_1^+ z} + A_2^+ e^{ik_2^+ z} \right) J_m(\gamma s) e^{im\phi + \lambda t} \\
u^+ &= \tfrac{1}{2} \left(A_1^+ e^{ik_1^+ z} + A_2^+ \frac{k_2^+}{i\gamma} e^{ik_2^+ z} \right) (J_{m+1}(\gamma s) - J_{m-1}(\gamma s)) e^{im\phi + \lambda t}, \\
iv^+ &= \tfrac{1}{2} \left(A_1^+ e^{ik_1^+ z} + A_2^+ \frac{k_2^+}{i\gamma} e^{ik_2^+ z} \right) (J_{m+1}(\gamma s) + J_{m-1}(\gamma s)) e^{im\phi + \lambda t}, \\
p^+ &= \frac{\lambda}{\gamma} A_1^+ e^{ik_1^+ z} J_m(\gamma s) e^{im\phi + \lambda t},
\end{aligned} \tag{6.2}
$$

to (6.1) for $z > 0$, and (letting $p \to \alpha p$ and $Re \to \alpha Re/\beta$) the separable solution for $z < 0$

$$
\begin{aligned}
w^- &= \left(A_1^- e^{ik_1^- z} + A_2^- e^{ik_2^- z} \right) J_m(\gamma s) e^{im\phi + \lambda t}, \\
u^- &= -\tfrac{1}{2} \left(A_1^- e^{ik_1^- z} + A_2^- \frac{ik_2^-}{\gamma} e^{ik_2^- z} \right) (J_{m+1}(\gamma s) - J_{m-1}(\gamma s)) e^{im\phi + \lambda t}, \\
iv^- &= -\tfrac{1}{2} \left(A_1^- e^{ik_1^- z} + A_2^- \frac{ik_2^-}{\gamma} e^{ik_2^- z} \right) (J_{m+1}(\gamma s) + J_{m-1}(\gamma s)) e^{im\phi + \lambda t}, \\
p^- &= -\frac{\alpha\lambda}{\gamma} A_1^- e^{ik_1^- z} J_m(\gamma s) e^{im\phi + \lambda t}.
\end{aligned} \tag{6.3}
$$

provided

$$
\begin{aligned}
k_1^+ &:= i\gamma, \qquad & k_2^+ &:= i\sqrt{\gamma^2 + \lambda Re} \qquad & \text{in} \quad z > 0, \\
k_1^- &:= -i\gamma, \qquad & k_2^- &:= -i\sqrt{\gamma^2 + \alpha\lambda Re/\beta} \qquad & \text{in} \quad z < 0
\end{aligned}
$$

where $J_m(s)$ is the Bessel function of the first kind with order m. Matching u, w, σ_{sz} and the jump condition on σ_{zz} at $z = 0$ gives (respectively)

$$
\begin{aligned}
A_1^+ + A_2^+ \frac{k_2^+}{i\gamma} + A_1^- + A_2^- \frac{ik_2^-}{\gamma} &= 0, \\
A_1^+ + A_2^+ - A_1^- - A_2^- &= 0, \\
2\gamma^2 A_1^+ + (2\gamma^2 + \lambda Re) A_2^+ - 2\beta\gamma^2 A_1^- - \beta(2\gamma^2 + \alpha\lambda Re/\beta) A_2^- &= 0, \\
(-\lambda^2/\gamma - 2\lambda\gamma/Re - \gamma^2 T + (1 - \alpha)) A_1^+ & \\
+ (-2\lambda/Re\sqrt{\gamma^2 + \lambda Re} - \gamma^2 T + 1 - \alpha) A_2^+ & \\
- (\alpha\lambda^2/\gamma + 2\beta\gamma\lambda/Re) A_1^- - 2\beta\lambda/Re\sqrt{\gamma^2 + \alpha\lambda Re/\beta}\, A_2^- &= 0
\end{aligned} \tag{6.4}
$$

(matching v and $\sigma_{\phi z}$ automatically follow from these). The requirement that the determinant of this 4×4 matrix vanishes yields the dispersion relation $\lambda = \lambda(\gamma, \alpha, \beta, T, Re)$. The remaining issue is the choice of γ which is how the sidewall boundary conditions enter. Only one condition can be imposed and this logically should be the inviscid criterion $u(1, \phi, z) = 0$ or

$$
J_{m+1}(\gamma) = J_{m-1}(\gamma) \tag{6.5}
$$

so that the flow does not penetrate the sidewalls. If $m = 0$, the boundary condition (6.5) simplifies to $J_1(\gamma) = 0$ and $v^+(s, \phi, z) = v^-(s, \phi, z) = 0$ since $J_{-m}(\gamma s) = (-1)^m J_m(\gamma s)$. Coincidentally $dw/ds = 0$ also at $s = 1$ since $dJ_0(\gamma s)/ds = -\gamma J_1(\gamma s)$ so that the separa-

		λ_0	λ_1
'exact'		1.437060×10^{-3}	2.990345×10^{-3}
20×20	H/R=5	1.437342×10^{-3}	2.959425×10^{-3}
20×40	H/R=10	1.437060×10^{-3}	2.990333×10^{-3}
20×60	H/R=20	1.437060×10^{-3}	2.990345×10^{-3}

TABLE 3. Leading growth rates λ_0 and λ_1 for a cylinder of radius = 3.15cm, upper fluid of golden syrup ($\rho_1 = 1.1\text{g/cm}^3$, $\mu_1/\rho_1 = 1200\text{cm}^2/\text{s}$) and lower fluid of silicone oil ($\rho_2 = 0.98\text{g/cm}^3$, $\mu_2/\rho_2 = 600\text{cm}^2/\text{s}$) so lowest roots $\gamma_0 = 3.83170597021$, $\gamma_1 = 1.84118378134$, $\alpha = 0.8909090889$, $\beta = 0.445454544469$, $Re = 0.14592144043$ and $T = 0$. The resolution 20×40 means $L = 20$ and $N = 40$, H/R refers to the cylinder height-to-radius aspect ratio, and 'exact' indicates the result from solving the separable solution (6.4) for an infinite cylinder.

ble solution (6.2) and (6.3) satisfies physically-plausible stress-free boundary conditions on the sidewall. Unfortunately this luck does not carry completely over to the $m \neq 0$ case because v is there non-vanishing. (6.5) again implies that $dw/ds = 0$ at $s = 1$ but now also $d(sv)/ds = 0$ at the sidewall which is a Navier slip condition. In terms of testing the code, this unusual combination of boundary conditions is, of course, not a problem as the same conditions can easily be imposed on the spectral expansion functions. In particular, we use

$$\Theta_n = \begin{cases} T_0(s) & n = 0 \\ T_{2n+2}(s) - \dfrac{(n+1)^2}{n^2} T_{2n}(s) & n = 1, 2, \ldots \end{cases} \tag{6.6}$$

so $d\Theta_n/ds|_{s=1} = 0$ for w^+ and w^- and create a new spectral basis function

$$\Psi_n = T_{2n+2}(s) - \frac{4(n+1)^2 + 1}{4n^2 + 1} T_{2n}(s) \qquad n = 0, 1, \ldots \tag{6.7}$$

so that $d(s\Psi)/ds|_{s=1} = 0$ to represent v^+ and v^-. The comparison of leading growth rates obtained from the separable solution and from the full numerical solution is excellent in both $m = 0$ and $m = 1$ cases: see Table 3.

Appendix C: Side-by-Side Fingering

This appendix extends the discussion in section 5 to consider fingering solutions where the fingers are both in contact with the tube walls. This is built around the side-by-side solutions discussed in K11 and introduces a new complication compared to the axisymmetric finger solutions: two geometrical parameters are needed to uniquely define the cross-sectional area of the solution and hence the flux (e.g. the intersection of Γ with the tube wall and the radius of curvature of Γ). Since there appears no rationale for determining how these two parameters evolve in a fingering solution, we impose a simple/plausible relationship between them to recover a one parameter of possible cross-sections to proceed as above. In the nomenclature of K11 (see figure 11), a reasonable choice is

$$\alpha = \frac{\pi}{4} \left(\frac{2\gamma}{\pi} \right)^{\delta} \tag{6.1}$$

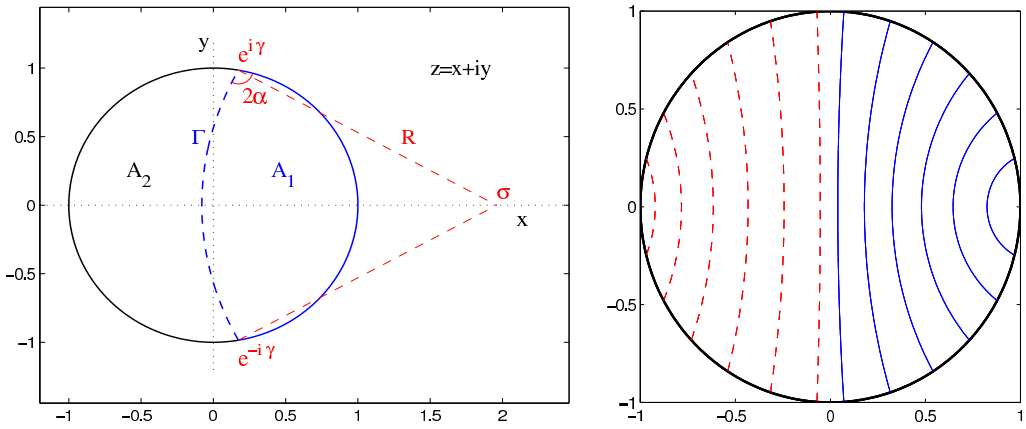

FIGURE 11. (a) The definitions of γ and α in the side-by-side solution from K11. (b) Cross-sections of Γ at $\gamma = (0.25, 0.5, 0.75, 1, 1.25$ and 1.5 for i) $\delta = 0.1$ ($x > 0$ solid blue lines) and ii) $\delta = 0.5$ ($x < 0$ dashed red lines).

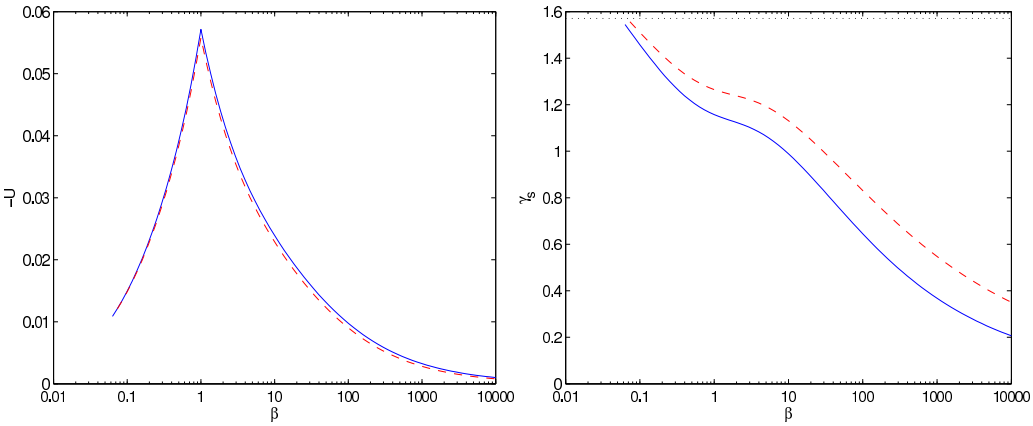

FIGURE 12. (a) The speed of the shock for the downward propagating finger as a function of β for the side-by-side finger solution with $\delta = 0.1$ (blue solid line) and $\delta = 0.5$ (dashed red line). (b) the shock position (angle) γ_s as a function of β for $\delta = 0.1$ (blue solid line) and $\delta = 0.5$ (dashed red line). Notice the lines are terminated when $\gamma_s \to \pi/2$ (marked as a dotted line).

where two choices for δ are considered: $\delta = 0.1$ and 0.5. This functional form has been designed so that $2\alpha > \gamma$ (the interface is convex) and $\alpha(\pi/2) = \pi/4$ so that the finger connects to the 'half and half' solution where Γ is a diameter. This latter feature allows us to just consider one finger simplifying the presentation. Figure 11 also shows what the corresponding cross-sections look like.

With (6.1) the angle γ plays the role of χ and we proceed as before albeit $Q_i = Q_i(\gamma, \alpha(\gamma))$ has to be calculated numerically (see K11). Figure 12 collects together the predictions for the descending finger of denser fluid (fluid 1) centred around $\gamma = 0$ (the corresponding predictions for the upward moving finger centred at $\gamma = \pi$ are contained under the transformation $\beta \to 1/\beta$). This shows that the shock location as defined by the angle γ_s approaches 0 as $\beta \to \infty$ which therefore represents the best hope of making contact with reality. The choice of δ does not seem to have much effect on the shock speed but does on the shock position.

Other types of fingering solutions can be constructed - e.g. fingering solutions where the fingers are displaced from the central axis which would involve eccentric core-annular

solutions - but again the fluxes are functions of two geometrical parameters and some arbitrary choice needs to be made (see Sweeney 2011 for more details).

7. References

Abarzhi, S.I. "Review of theoretical modelling approaches of Rayleigh-Taylor instabilities and turbulent mixing" *Phil. Trans. Roy. Soc.* **368**, 1809–1828 (2010).

Arakeri, J.H., Avila, F.E., Dada, J.M. & Tovar, R.O. "Convection in a long vertical tube due to unstable stratification- A new type of turbulent flow?" *Current Science* **79**, 859-866, 2000

Arnett, W.D., Bahcall, J.N., Kirshner, R.P. and Woosley, S.E. "Supernova 1987 A" *Annu. Rev. Astron. Astrophys.* **27**, 629 (1989).

Batchelor, G.K. and Nitsche, J.M. "Instability of stratified fluid in a vertical cylinder" *J. Fluid Mech.* **252**, 419–448 (1993)

Beckett, F., Mader, H.M., Phillips, J.C., Rust, A. & Witham, F. "An experimental study of low Reynolds number exchange flow of two Newtonian fluids in a vertical pipe." *J. Fluid Mech.* 2011

Bellman, R. & Pennington, R.H. "Effects of surface tension and viscosity on Taylor instability" *Q. Appl. Maths* **12**, 151-162 (1954).

Chandrasekhar, S. "Hydrodynamic and Hydromagnetic Stability" Oxford, Clarendon Press 1961.

Chen, C.Y. and Meiburg, E. "Miscible displacements in capillary tubes. 2. Numerical simulations" *J. Fluid Mech.* **326**, 57-90 (1996)

Drazin, P.G. & Reid, W. "Hydrodynamic Stability" Cambridge University Press 1981.

Duprez, M. "Sur un cas particulier de l'équilibre des liquides" *Nouv. Mém. Acad. Belg.* (1851 & 1854)

Hinds, W., Ashley, A., Kennedy, N. and Bucknam, P. "Conditions for cloud settling and Rayleigh-Taylor instability" *Aerosol Sci. Technol. 36*, 1128 (2002).

Huppert, H.E. & Hallworth, M.A. "Bi-directional flows in constrained systems" *J. Fluid Mech.* **578**, 95-112, 2007.

Jacobs, J.W, Bunster, A., Catton, I. and Plesset, M.S. "Experimental Rayleigh-Taylor instability in a Circular Tube" *Trans. ASME I: J. Fluids Engng* **107**, 460–466 (1985)

Jacobs, J. W. and I. Catton, I. "Three-dimensional Rayleigh-Taylor instability Part 2. Experiment" *J. Fluid Mech.* **187**, 353-371 (1988).

Kerswell, R.R. and Davey, A. "On the linear instability of elliptic pipe flow" *J. Fluid Mech.* **316**, 307-324, 1996.

Kerswell, R.R. "Exchange flow of two immiscible fluids and the principle of maximum flux" *J. Fluid Mech.* 2011 (referred to as K11 in the text).

Kuang, J., Maxworthy, T. and Petitjeans, P. "Miscible displacements between silicone oils in capillary tubes" *Eur. J. Mech. B* **22**, 271-277 (2003).

Lindl, J.D., McCrory, R.L. and Campbell, E.M. "Progress toward ignition and burn propagation in inertial confinement fusion" *Phys. Today* **45**, 32, (1992).

Malekmohammadi, S., Carrasco-Teja, M., Storey, S., Frigaard I.A. and Martinez, D.M. "An experimental study of laminar displacement flows in narrow vertical eccentric annuli" *J. Fluid Mech.* **649**, 371-398 (2010)

Matson, G.P. & Hogg, A.J. "Viscous exchange flows" *Phys. Fluids* **24**, 023102, 2012.

Maxwell, J.C. Scientific papers vol II 1890 (ed. W.D. Niven), Cambridge University Press, p 587.

Petitjeans, P. and Maxworthy, T. "Miscible displacements in capillary tubes. 1. Experi-

ments" *J. Fluid Mech.* **326**, 37-56 (1996).
Rayleigh, J.W.S. "Investigation of the character of the equilibrium of an incompressible heavy fluid of variable density" *Proc. Lond. Math. Soc.* **14**, 170-177 (1883)
Sharp, D.H. "An overview of Rayleigh Taylor instability" *Physica D* **12**, 3–18 (1984).
Stevenson, D.S. and Blake, S. "Modelling the dynamics and thermodynamics of volcanic degassing" *Bull. Volcanol.* **60**, 307–317 (1998).
Sweeney, H. "The Rayleigh-Taylor instability in a cylinder: linear instability analysis and long-time solutions" MSc. thesis, School of Mathematics, University of Bristol, May 2011.
Taylor, G.I. "The instability of liquid surfaces when accelerated in a direction perpendicular to their planes" *Proc. Roy. Soc. Lond.* **A 201**, 192-196 (1950)
Vanaparthy, S.H., Meiburg, E. and Wilhelm, D. "Density-driven instabilities of miscible fluids in a capillary tube: linear stability analysis" *J. Fluid Mech.* **497**, 99-121 (2003).
Vanaparthy, S.H. and Meiburg, E. "Variable density and viscosity, miscible displacements in capillary tubes" *Eur. J. Mech. B* **27**, 268-289 (2008).
Whitehead, J.A. and Luther, D.S. "Dynamics of laboratory diaper and plume models" *J. Geophys. Res.* **80**, 705 (1975).
Wooding, R.A. "The stability of a viscous liquid in a vertical tube containing porous material" *Proc. R. Roy. Lond.* **252**, 120 (1959).
Wilkinson, J.P. and Jacobs, J.W. "Experimental study of the single-mode three-dimensional Rayleigh-Taylor instability" *Phys. Fluids 19*, 124102 (2007).
Yih, C.-S. *Stratified Flows* 1980 Academic Press, New York.
Yu, H. and Livescu, D. "Rayleigh-Taylor instability in cylindrical geometry with compressible fluids" *Phys. Fluids* **20**, 104103 (2008).

video caption for supplementary material

This video shows the motion induced by overturning a 15 cm long, 6.3 cm diameter glass cylinder which is filled 50:50 with golden syrup ($\rho_1 = 1.1$ g/cm^3, $\nu_1 = 1200$cm^2/s) and silicone fluid ($\rho_2 = 0.98$g/cm^3, $\nu_2 = 600$cm^2/s). The video starts just as the motion begins which is ≈ 2 secs. after overturning. Note the creation of a pair of cusps in the middle of the cylinder.